DEVELOPMENT OF A LIGHTWEIGHT, ENERGY ABSORBING SOFT-LANDING SYSTEM FOR ROBOTIC PROBES

Scott Cooper, Gordon Maahs, Devamanohar Ponnusamy

Johns Hopkins University Applied Physics Laboratory
11100 Johns Hopkins Road
Laurel, MD 20723 USA
Email: scott.cooper@jhuapl.edu

ABSTRACT

For more than 40 years, robotic probes have been landing on surfaces of extraterrestrial bodies. Recent mission concepts continue to place a high value on robotic solar system surface exploration. Engineers from NASA/MSFC and JHU/APL are developing a lunar lander design to support a variety of mission concepts. In support of the Robotic Lunar Lander (RLL) risk reduction program, the team is building an analogous full-scale lander testbed for an Earth-based terminal descent and landing demonstrator.

The RLL mechanical team has focused on developing a robust, lightweight soft-landing system for these lander concepts. This paper provides an overview of the baseline landing system design and the concept development process. Results of component and subassembly analysis and development testing are discussed. The impact of the current effort, as related to future design optimization, is also discussed.

1. INTRODUCTION

For the past several years, NASA has been studying mission concepts for sending robotic landers to the Earth's moon. These studies have focused on a mixture of human precursor activities and pure scientific investigations. Mission parameters for these studies have varied greatly, with various target landing sites, mission durations, and instrument payload suites. A significant number of studies were compiled by the Robotic Lunar Lander (RLL) team, comprised of engineers from NASA's Marshall Space Flight Center (MSFC) in Huntsville, AL and the Johns Hopkins University Applied Physics Laboratory (JHU/APL) in Laurel, MD.

In 2009, the team focused on mission concepts centered on a lander built to deliver instruments as a part of the International Lunar Network (ILN) [1]. A series of mission-level trades helped shape a baseline mission architecture, which was further defined by lander subsystem trades and conceptual design (See Fig. 1). Recently, the team has focused on a Lunar Polar Volatiles Explorer (LPVE) mission, using a baseline lander concept from the ILN studies and modifying the architecture where required [2].

Fig. 1. ILN lander concept

Throughout the mission concept study period, the team has spent considerable effort to develop and demonstrate aspects of the conceptual design seen as higher risk to the mission. A major risk reduction activity involves building a hardware demonstration of the terminal descent phase of the landing. The team is currently building an autonomous, Earth-based free-flying vehicle that will demonstrate lander control algorithms for the critical last minute of the mission prior to landing. The vehicle, known as the Warm Gas Test Article (WGTA), will incorporate flight-like guidance, navigation and control (GNC) sensors on a lander derived from the RLL baseline design. The WGTA will use a hydrogen peroxide propulsion system with off-the-shelf power and communication components and a GPS-based "truth" system for evaluating vehicle performance.

The RLL mechanical team is leveraging the task of designing and building the WGTA to help develop a

robust landing system for future missions. Design and development activities are structured to apply to a variety of space-based missions, as well as satisfy the WGTA requirements. Special design accommodations for the WGTA system are noted for parallel or subsequent design, analysis and test. The goal for the team is to develop a robust, lightweight landing system that meets the requirements outlined in Section 2. Prototype component testing and analysis of the system indicate the design will meet this goal.

2. LANDING SYSTEM REQUIREMENTS AND TRADES

Throughout the ILN and RLL effort, the design team has collected many requirements from a variety of mission concepts and instrument payloads. Over the course of several studies, these requirements (see Sect. 2.1) were used to inform a series of trades (see Sect. 2.2). As many mission requirements are similar, the progression of trades led to a common baseline system architecture for most of the mission concepts studied. As the system architecture evolved, the team was able to establish more detailed subsystem-level requirements (see Sect. 2.3), which the mechanical team used for a detailed landing system design.

2.1 Mission Requirements

Several mission requirements were critical to the landing system architecture trades. First, the target in all RLL concept studies has been the Earth's moon. The lack of an atmosphere eliminates the opportunity to use aerobraking prior to landing, but also eliminates concerns about aeroshells, aeroheating, etc. during descent. Second, with the extensive and detailed surface mapping of the moon from missions such as the Lunar Reconnaissance Orbiter (LRO) and Chandrayaan-1, a priori knowledge of the approximate landing site parameters was assumed. While the landing site is dependent on the mission, areas with minimal distribution of rocks and craters greater than 30 cm and gentle overall slopes of less than 10 degrees comprised the set of landing hazards. In some cases, these areas could be found with relative ease, and the targeted landing site could be up to 100 km wide. In other areas, the desire to land at a more controlled location, or the presence of hazards in the vicinity of the landing target required an on-board system to provide more precise navigation. Once the lander arrives at the landing site, the orientation of the lander must be controlled. For communications, thermal control, and some science requirements, a particular side of the lander was required to point toward a lunar pole. In addition to clocking of the lander, in some missions a controlled slope of the lander decks was required.

2.2 System Architecture Trades

An important trade for the lander system architecture was the type of landing system. A comprehensive survey of previous lander concepts, along with a concerted effort to explore many options, produced a set of possible lander configurations. Landing systems considered fell into two broad categories, each comprised of subcategories.

- Soft Landers
  - Legged landers (Apollo, Phoenix)
  - Platform or pallet landers (Surveyor)
  - Airbag landers (MER)
- Hard Landers
  - Penetrators
  - Impactors

In an effort to keep the lander concepts relevant to multiple mission concepts, a wide range of payload and system masses was considered. The resulting lander concept should perform a variety of tasks, and be launched on a variety of launch vehicles. Due to the sensitivity to shock of the seismometer in the ILN mission and the general lack of success of penetrator missions, the hard lander category was eliminated fairly early. Airbags were eliminated due to the need to control landing orientation, concern over the deflated airbag restricting instrument access to the lunar surface, and overall system mass. Low mass became the driving requirement in many trade downselects. While the platform lander concept seemed very promising, practicalities of the lander system requirements, such as ground clearance for thrusters and control of landing orientation eventually eliminated the pallet concept. The legged lander concept would be the baseline design.

2.3 Landing System Requirements

Other system requirements that influence the design of the landing system are the set of parameters that bound the kinematic state of the lander at touchdown. Working together, the mechanical and GNC subsystem teams established the requirements in Table 1 for the lander at touchdown. These requirements are also similar to landing design requirements from previous lunar missions.

Table 1. Landing System Touchdown Requirements

Requirement	RLL	WGTA
Vertical rate (m/sec)	0.0 - 1.25	0.0 - 4.0
Lateral rate (m/sec)	0.0 - 1.25	0.0 - 1.5
Lander angle (deg)	0.0 - 10.0	0.0 - 10.0
Angular rate (deg/s)	0.0 - 5.0	0.0 - 10.0
Free fall height (m)	0.0 - 1.25	0.0

The different values for vertical rate and drop height between the RLL and WGTA reflect the difference in planned landing operations. Both landers intend to descend at 1.0 m/sec during the terminal descent phase of landing. At approximately one meter above the surface, the RLL lander intends to shut off its engines to reduce engine plume effects on the surface. The WGTA engine shut-off is trigged when the landing leg deflects and trips the ground contact sensor. Free fall of the WGTA was avoided because of the much higher gravity on Earth, which leads to much higher impact velocities. Using Eq. (1), where V_f and V_0 are final and initial velocities, g is acceleration due to gravity, and h is drop height, the maximum impact velocity for the RLL on the moon is 2.4 m/sec.

$$V_f^2 = V_0^2 + 2gh \tag{1}$$

Although the WGTA does not plan to free fall to the surface, the WGTA vertical rate requirement is significantly higher than the RLL to account for landing anomalies as the control and landing systems are developed and tested. Another unique requirement for the WGTA landing system is that it be reusable without servicing legs after each landing.

3. BASELINE LANDING SYSTEM CONCEPT

Once the baseline system architecture and high-level requirements were defined, the RLL mechanical team could begin defining the details of the landing system. There are many successful lander programs from which to build upon. Missions such as Surveyor, Apollo, Viking, and Phoenix provided valuable lessons learned to the design of the RLL landing system. Consistent with past robotic landers, the RLL landing system contains only three legs, primarily due to mass constraints.

3.1 Leg Configuration

Two basic leg configurations were considered: cantilever and inverted tripod, each with three members attached to the lander and a footpad at the base (see Fig. 2). In the early RLL concepts, the cantilever leg design was chosen, primarily based on the extensive documentation from Apollo landers. However, as the overall lander design matured, a leg configuration trade showed the inverted tripod design to transmit load more efficiently. Although the inverted tripod design requires longer secondary legs and produces slightly higher axial loads in the primary leg, it also avoids the significant primary leg bending moment in the cantilever design.

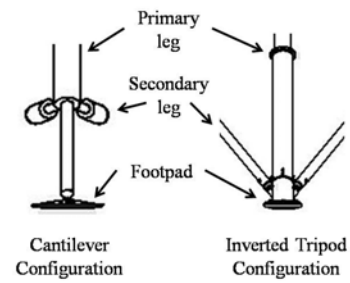

Fig. 2. Leg configurations

Many previous landers had to accommodate deployable legs, but the majority of the RLL concepts did not have tight volume constraints for the legs. To keep the design simple and mass lower, a leg deployment feature was not included in the baseline design.

3.2 Energy Absorption

Another leg configuration trade was focused on the method of absorbing the landing impact energy. To prevent damage to the lander and its components, a requirement to limit quasi-static acceleration of the lander center of gravity (CG) to 5G was assumed. Hydraulic and pneumatic systems were avoided to reduce assembly complexity and mass. A crushable aluminum honeycomb cartridge, similar to the Apollo design, was an easy choice based on its previous success, well-documented, linear behavior, and low mass. In the interest of fully exploring the trade space, low density aluminum foam was also considered. However, aluminum foam testing showed it to be expensive and not as predictable as honeycomb. The ability to specify the foam's density and to apply load in many directions may make it attractive for other applications, but the aluminum honeycomb was eventually chosen as the baseline.

The major differences between the RLL and WGTA landing system are the WGTA's higher impact velocity and its requirement that the system be reusable without service. To help relieve the effects on the leg design of the increased impact energy, the WGTA quasi-static CG acceleration limit was increased to 10G. The durability required of the WGTA structure to withstand many landing cycles means significant structure mass would not be added to the system to meet the 10G requirement.

Crushable honeycomb will not satisfy the WGTA reusability requirement, so the team looked for a honeycomb replacement for the Earth-based vehicle. A hydraulic damper (see Fig. 3) from Enidine Inc. was selected that was relatively low mass and would provide the energy absorption required by the WGTA. An attractive feature of the damper is its adjustable damping knob, which allowed the team to choose a damper and collect performance data before the final damping requirements were established. Significant testing of the damper helped the team determine its performance over a range of impact velocities and lander masses. Although the damper's performance is highly non-linear, it allows the design to meet the reusability requirement. However, testing revealed the damper could not fully support the higher WGTA landing rates. Consequently, a honeycomb cartridge is mounted in-line with the damper. The honeycomb crush strength is chosen to crush in only "off-nominal" landings, defined as 4.0 m/sec vertical rate and > 5 deg lander angle. This design will further protect the vehicle during development flights, and will provide the team experience using different energy absorbers in series. The accommodation of the damper in the leg design allows the damper to be completely replaced by honeycomb with appropriate crush strength if a flight-like honeycomb landing demonstration is desired.

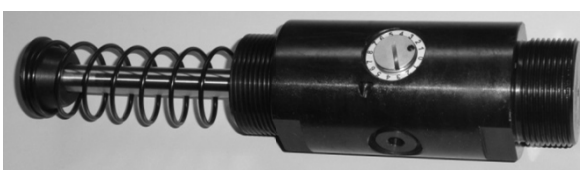

Fig. 3. WGTA leg damper

3.3 Landing Stability

Although the design of landing systems was new to the RLL mechanical team at the beginning of the effort, many aspects of the landing system design are similar to other space vehicle mechanical design concepts. Landing stability, however, presented a much steeper learning curve. The team conducted extensive research into the methods used to predict and the ultimate flight performance of past lander missions. The Surveyor missions collected interesting data on landing dynamics and even conducted several experiments related to landing and surface impact. The most useful collection of analysis and test methods came from Apollo-era documents.

The team initially sized lander legs using simplified kinematic equations from work performed in the 1960's [3]. A landing stability plot for the WGTA design is shown in Fig. 4. This plot is for the 2-and-over case, where the lander initially impacts on two legs and flips over. The 2-and-over case is the least stable case for most landing conditions. The plot shows the stability boundaries for the unfueled and fully fueled WGTA, where the mass and CG location are adjusted accordingly. Landing conditions with a particular pairing of lateral and vertical velocities will be stable if they are located to the left of a plot. The WGTA landing conditions are shown within the shaded area, making the WGTA stable for its landing requirements.

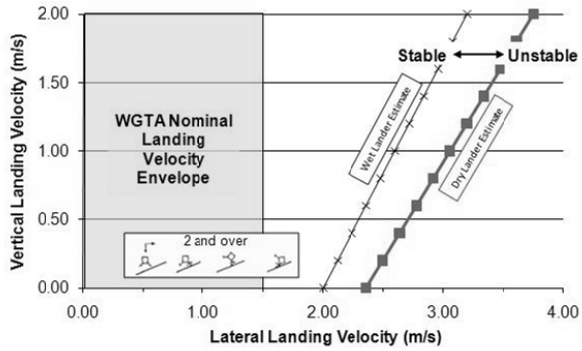

Fig. 4. WGTA landing stability

Later in the Apollo program, these methods were shown to be inadequate for predicting stability in certain touchdown conditions [4]. The Apollo team ultimately developed much more complex numerical simulations of the touchdown dynamics which were later validated through testing [5]. Because the Apollo work concentrated on four-legged landers and the RLL lander only had three legs, the simplistic stability method was used at the conceptual design level. The RLL team is working to incorporate updated kinematic analysis tools to predict the landing system behavior.

3.4 Baseline Leg Design Summary

The resulting baseline landing system design consists of three subassemblies, each containing a primary leg and two secondary legs in an inverted tripod arrangement. A footpad is attached at the base of the leg assembly. Fig. 5 shows the WGTA leg assembly attached to a portion of the WGTA lander structure.

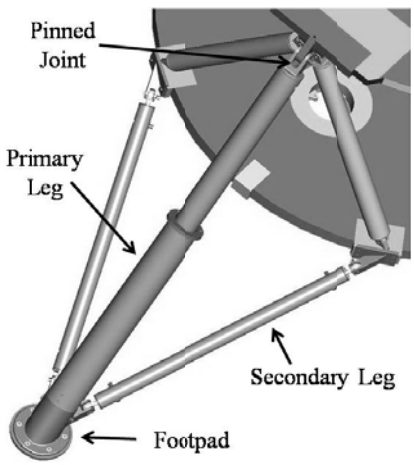

Fig. 5. WGTA landing leg assembly

The primary leg contains an aluminum honeycomb cartridge, which is sized based on landing parameters and vehicle mass. The damper, described in Sect. 3.2, is included in series with the honeycomb for the WGTA leg design (See Fig. 6). The secondary legs do not contain energy absorbing material, but the option for a plastically deformable load limiter at the lander attachment locations is still being examined. Each end of the three leg members contains a spherical joint, with the exception of the primary leg attachment to the lander, which is a pinned joint. When the vehicle lands on the footpad, the primary leg is compressed as the honeycomb crushes and the lander decelerates. As the primary leg shortens, the three leg members rotate about the secondary leg attachments to the lander. The spherical joints at the ends of the members are critical to allowing this motion and prevent binding of the assembly.

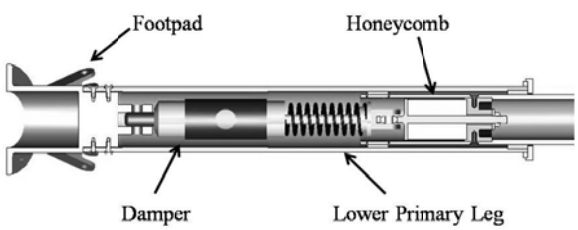

Fig. 6. WGTA primary leg assembly cross-section

The RLL version of the leg assembly has proven to be a robust design, applicable to a range of missions. Using the experience gained through testing and analysis thus far, the team has identified the driving factors for the landing system design. The team has been able to scale the leg design, based on overall vehicle size, system mass, and landing conditions. Leg geometry can be adjusted to improve landing stability or satisfy a specific ground clearance or ground proximity requirement, depending on mission parameters.

4. LEG TESTING

As a system, the lander legs are complex assemblies, therefore performance over a range of conditions is difficult to predict. The individual components and subassemblies are similar to other spacecraft structures and mechanisms and well understood by the team. The crushable honeycomb cartridge is the exception within the group. Early leg designs relied heavily on honeycomb vendor performance data, but the team wanted to gain experience with the testing and performance of honeycomb crushing.

Using requirements from Section 2, the team performed a rough sizing of the honeycomb required for the RLL leg system. The sizing process involves calculating the minimum stopping distance required to limit the lander deceleration using Eq. (2), where s is crush stroke and G is the lander G limit.

$$s = \frac{h}{G-1} \tag{2}$$

When the lander mass, impact velocity, minimum stopping distance, and honeycomb cartridge diameter are known, the required honeycomb crush strength, f_{CR} is found from Eq. (3), where A_{CR} is the area of the honeycomb footprint.

$$f_{CR} = \frac{mg(h+s)}{A_{CR}s} \tag{3}$$

Initial honeycomb sizing calculations indicated that honeycomb crush strength in the 100 psi range would be a good starting point. The RLL team fabricated 7.6 cm square test coupons from a sheet of 7.6 cm thick Hexcel CRIII 1/8-5052-3.1 honeycomb (3.1 pcf density, 900 kPa crush strength). Coupons were tested at a range of loading rates and in single and stacked configurations. In all testing, the honeycomb crush test results were very linear and matched well with the vendor specifications.

4.1 Quasi-static honeycomb testing

Testing began with simple honeycomb crushing in an Instron at a low loading rate. The initial peak in crush force is perhaps the only slight drawback to using honeycomb for energy absorption (see Fig. 7). However, as noted in the vendor literature [6], the peak can be eliminated if the honeycomb is first "precrushed," or loaded prior to use to overcome the honeycomb compressive strength and initiate cell buckling. Vendor guidelines suggest allowing 3-6 cm for precrush height, but test data indicates 2-3 mm of precrush is sufficient for the core density tested. The Instron machine proved very convenient for

precrushing honeycomb coupons and all subsequent test coupons were precrushed prior to test.

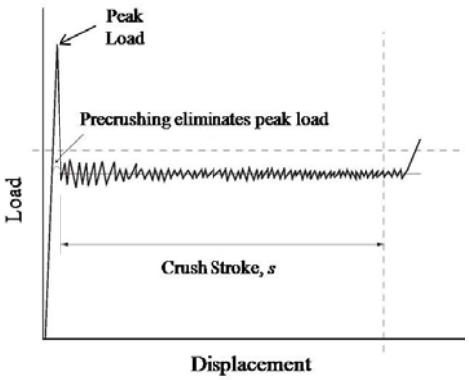

Fig. 7. Vendor honeycomb loading curve [6]

A series of precrushed coupons was tested at loading rates of 0.25, 1.3, and 25 mm/min. Coupon test data compared well with the available vendor data. The honeycomb exhibited consistent strength throughout the crush stroke. The measured values were approximately 5.4 kN, and the expected force was 5.2 kN. However, the expected force is highly dependent on the dimensions of the coupons, which were not measured closely for these tests. Additionally, the data shows two stacked precrushed coupons resulted in crush strength equivalent to the single coupon through twice the crush stroke (see Fig. 8). The average coefficient of variation (CV) in load within single samples was less than 1.1%, and the average CV between five different coupons was less than 1%.

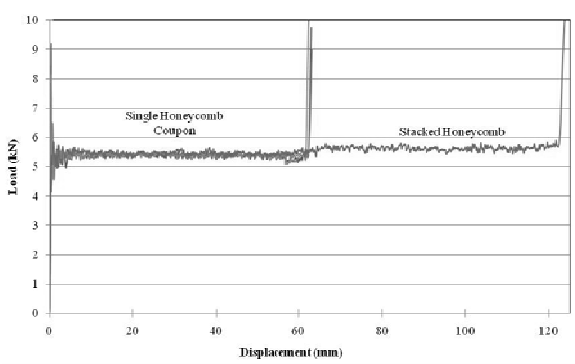

Fig. 8. Quasi-static loading test data

4.2 Dynamic honeycomb testing

After validating the core precrush process and measuring quasi-static crush performance, testing progressed to a dynamic loading, more representative of landing conditions. The first dynamic testing was performed on an Instron 8821S system (see Fig. 9). Test coupon size was reduced to a 5 cm square due to Instron load limitations. Coupons were precrushed and tested at rates of 2.0, 2.5, and 3.0 m/sec. A rolling point average was used to filter the test data to eliminate ringing.

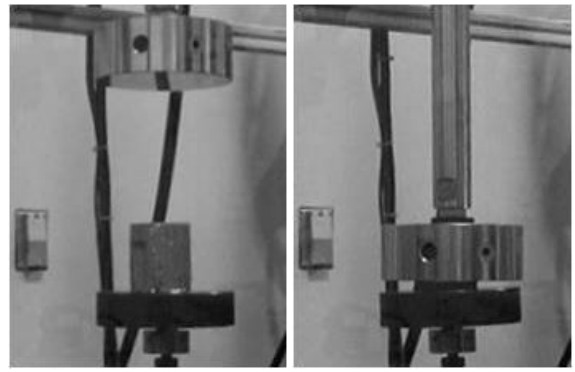

Fig. 9. Dynamic test set-up, before and after

Crush strength was consistent for each loading rate and very similar across all loading sets. The measured values were approximately 2.4 kN, and the expected value was 2.3 kN. The dynamic testing showed a slight increase in crush strength as the coupon was crushed, which is consistent with vendor literature. Stacked coupons performed similarly to the single coupons, with twice the stroke. The complication in the dynamic testing was that the test set-up was not able to apply a consistent loading rate throughout the crush stroke. This is obvious in the data in Fig. 10, where the initial loading rate is set at 3.0 m/sec, but the rate decreases dramatically as the honeycomb begins to crush. The dynamic testing gave the team more confidence in understanding the honeycomb behavior, but still wanted a test set-up that could reproduce landing conditions more accurately.

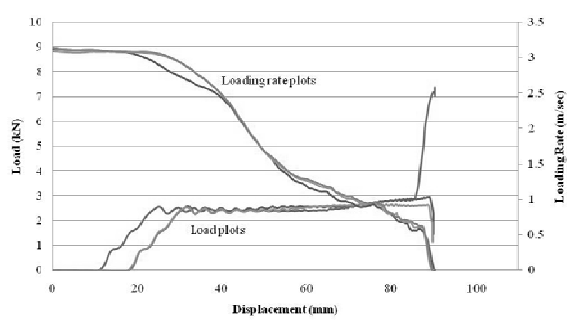

Fig. 10. Dynamic loading data

4.3 Drop testing

To provide a more realistic test set-up that could be used throughout the leg development effort, the team constructed a simple test rig to simulate landing impact (see Fig. 11). The rig is based on a weight training machine concept and consists of a carriage to hold weights and two vertical guide rails on which the carriage can be raised and lowered. The carriage is raised by a ratcheting crank and pulley system and held

suspended with a quick release latch. When the latch is opened, the carriage falls and lands on a strike plate, which holds a force transducer at the point of impact. By varying the drop height and the mass on the carriage, a range of impact energy is applied to the test article. In addition to the force tranducer, an accelerometer is mounted to the carriage to measure deceleration of the test mass. The motion of the test article is also recorded with a high speed camera system. Video analysis software identifies targets on the article and a post processing of the video yields the position, velocity and acceleration of the target points throughout its descent.

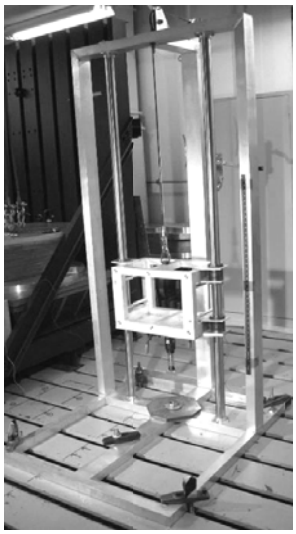

Fig. 11. Drop test fixture

The drop test set-up was first verified by crushing several honeycomb coupons and comparing the drop test data to the Instron test data. The left picture in Fig. 12 shows a bare 5 cm square honeycomb coupon prior to crushing in the drop test fixture.

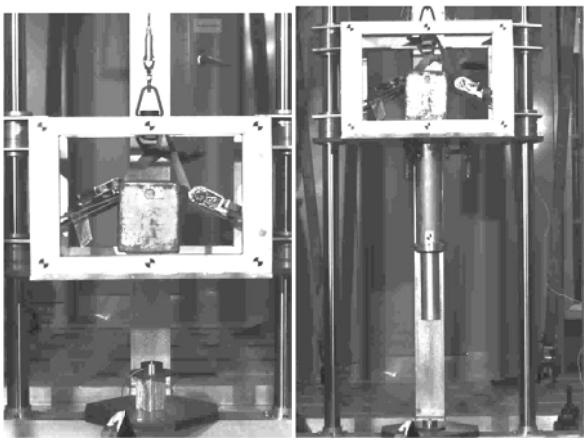

Fig. 12. Honeycomb testing on drop test fixture

The last configuration of initial testing is shown on the right of Fig. 12. A 5 cm square honeycomb coupon with 900 kPa crush strength is mounted inside a mockup of a primary leg, which is attached to the drop test carriage. The mass of the fixture is 49.9 kg, and the carriage is dropped from a height of 15 cm. This test provided the final validation of the test set-up and the ability to predict honeycomb energy absorbing performance. Measurements from this test are plotted in Fig. 13. Position and velocity of the carriage are processed with a low pass filter by the imaging system, and force at impact data is unfiltered from the force transducer. Accelerometer data was exceedingly noisy, and is not shown here. Table 2 compares the measured data to predictions using Eq. (1) to calculate impact velocity and Eq. (3) to solve for stopping distance (crush stroke). The impact velocity and stopping distance correlation is within the measurement error of the test data. Crush force prediction is close, but may require more testing and transducer calibration to explain the difference.

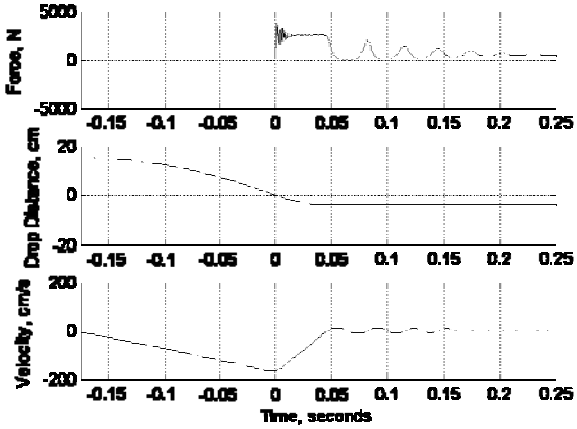

Fig. 13. Sample honeycomb drop test data

Table 2. Drop Test Predictions and Measured Values

	Predicted	**Measured**
Impact Velocity (m/sec)	1.74	1.67
Crush force (kN)	2.3	2.6
Stopping distance (cm)	4.12	3.88

Once the honeycomb behavior was understood, the team switched focus to developing the WGTA landing system. The drop test set-up proved to be critical to characterizing the WGTA damper behavior at various damping settings and loading conditions. A damper test unit was attached to the carriage and dropped from several heights and with a range of mass in the carriage. Data from a representative damper test is shown in Fig. 14. The sets of damper test data were compiled and used to help the team determine which damper setting was appropriate for the range of WGTA landing conditions. Further testing was focused on measuring damper performance at the chosen setting, which is setting “5.” This data was used to calibrate a mathematical model of the damper that could be used

to simulate WGTA landing performance with the damper installed.

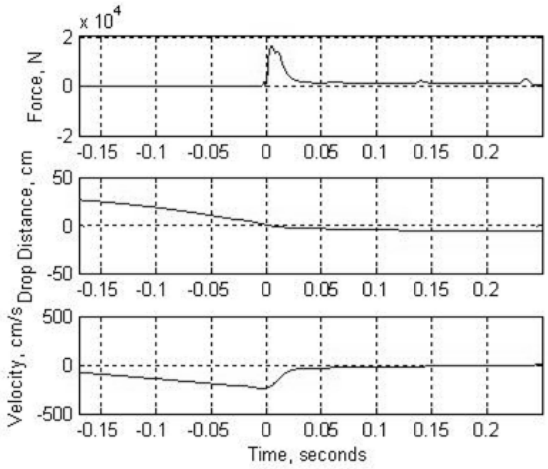

Fig. 14. Damper test data

5. LANDING SIMULATION AND ANALYSIS

Landing system analysis has the primary goal of verifying the WGTA leg assembly design, for both dynamic performance and component stress. The longer term goal is to develop a set of tools to optimize the landing system for various missions.

5.1 Dynamic modeling

To model dynamic performance of the landing system, the team chose Adams kinematic analysis software from MSC Corporation. The WGTA primary structure is represented as a pair of rigid decks with the vehicle mass located at the CG (see Fig. 15). Each leg member is modeled as a rigid bar with the appropriate end attachments. A contact function controls each footpad's interaction with the landing surface. A force-velocity function is inserted along the primary leg axis to simulate the energy absorbing component. For early model development, the force-velocity function represented only a honeycomb cartridge, for simplicity.

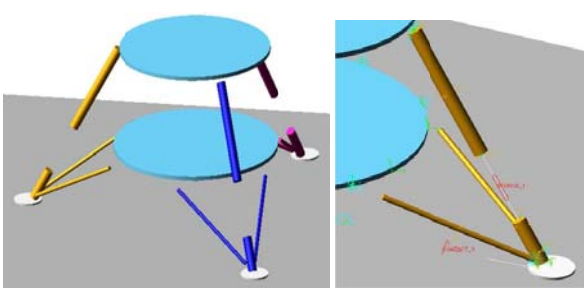

Fig. 15. Adams lander and lander leg models

Using the leg assembly model with honeycomb energy absorption, the predicted performance of the RLL vehicle for a landing case with no angles (simultaneous contact of 3 feet) is shown in Fig. 16. The model requires improvement and test validation (see Sect. 6), but the basic desired characteristics are apparent and are similar to predictions based on Eqns. (2) and (3). The quasi-static acceleration of the vehicle CG is limited to 4.8G by a honeycomb crush stroke of 4.8 cm. One feature for investigation is the oscillatory behavior of the CG location. This most likely indicates the Adams ground contact function is too "springy" and requires adjustment.

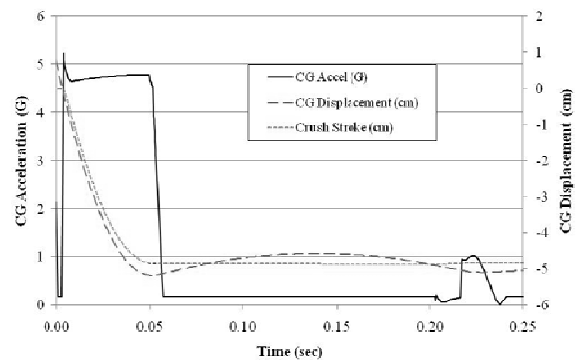

Fig. 16. Adams RLL landing simulation results

The unfortunate complication of the WGTA analysis was the difficulty in representing the non-linear behavior of the damper. With considerable effort, the damper force-velocity test data, described in Sect. 4.3, was converted into an Adams function. The function was verified by creating an Adams model of the damper test set-up and reproducing results from several test cases. A comparison of the Adams function prediction and the measured test data for a test case is shown in Fig. 17.

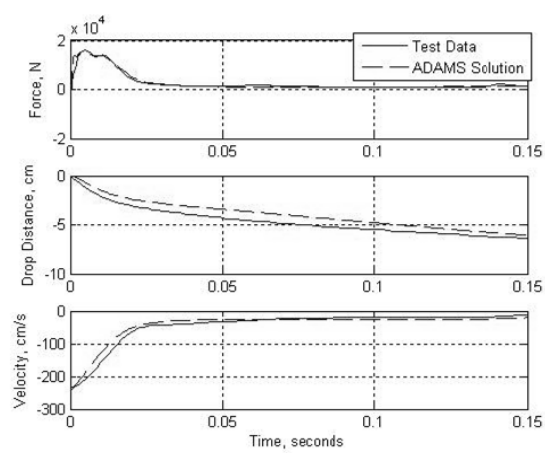

Fig. 17. Adams damper function validation

With a verified representation of the damper in Adams, the remaining step in the WGTA dynamic analysis was to use the Adams model to predict performance with a variety of initial conditions. Parameters such as CG

acceleration, velocity and position, force in each leg member, and primary leg stroke and angle were recorded for landing conditions across the ranges shown in Table 1. A plot of predicted landing performance is shown in Fig. 18. The non-linear behavior of the damper is apparent in the "2 hump" CG acceleration, rather than the "step function" in Fig. 16. From the simulation results the force in each leg is compiled for the various cases and enveloping leg forces are used to evaluate component stress in the legs as well as at the leg attachments to the vehicle structure (see Sect. 5.2).

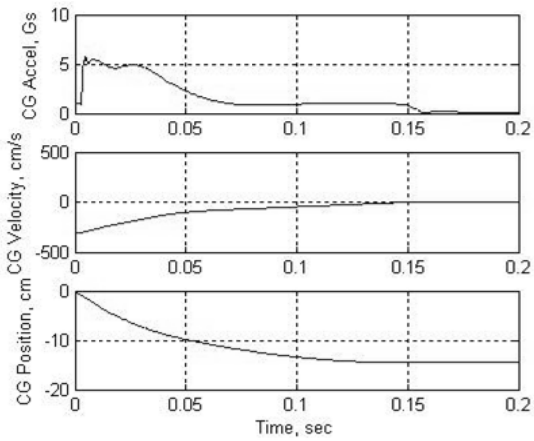

Fig. 18. Adams WGTA performance prediction

The team has made substantial progress toward developing a landing simulation tool. As testing progresses to more representative components and higher levels of assembly (see Sect. 6), the Adams model will evolve. Further model comparisons and correlation to test results will continue to enhance the simulation. Additionally, including an elastic representation of the vehicle and the leg members would further improve the model's predictions.

5.2 Component stress

A goal of the leg design effort is to develop a system that will decouple lander design loads from changing lander parameters and conditions. Within a certain set of requirements, the maximum lander interface loads could be established and the vehicle structure designed accordingly. As landing conditions are defined or changed, the leg design could be modified to accommodate the differences and limit the landing loads as specified. The key to this approach is to understand the leg design well enough to determine what modifications are required and how the system will react to the modifications. Dynamic performance is one part of this process, but predicting component loads and stresses is equally important. In addition, a detailed analysis can support design modifications to reduce component mass and optimize mass efficiency.

The team used preliminary estimates and engineering judgement to establish interface loads of 22.2 kN and 11.1 kN at the primary and secondary legs, respectively, for preliminary design activities. Landing simulations described in Sect. 5.1 proved the enveloped loads were below these design values. Due to the repetitive testing the legs will have to endure, conservative design loads seemed appropriate.

A finite element model of the leg assembly was created in FEMAP and analyzed in MSC/Nastran for various landing geometries. Table 3 summarizes the loading conditions. The ground impact load in each case was chosen to develop 22.2 kN force in the primary leg.

Table 3. Leg loads from Adams model

Case #	Landing angle (deg)	Rotation about	Ground impact load (kN)	Primary joint (kN)	Secondary strut #1 (kN)	Secondary strut #2 (kN)	Beam moment (N-m)
1	0	—	11.9	22.4	7.5	7.5	4
2	10	+Y, Side	12.3	22.4	10.1	4.6	4
3	10	-X, Out	13.5	22.3	5.7	6.4	4
4	10 each	X & Y	11.3	22.4	11.3	5.8	3
Max-Max			13.5	22.4	11.3	7.5	4

Detailed component stress analysis was conducted for each of the leg parts, and margin tables were created for the worst loading case for each part. A stress contour plot for the lower portion of the primary leg is shown in Fig. 19. Stress margins for the lower leg and foot are calculated in Table 4. The driving load case for the leg is load case #2 (see Table 3). However, the driving case for the foot is load case #4.

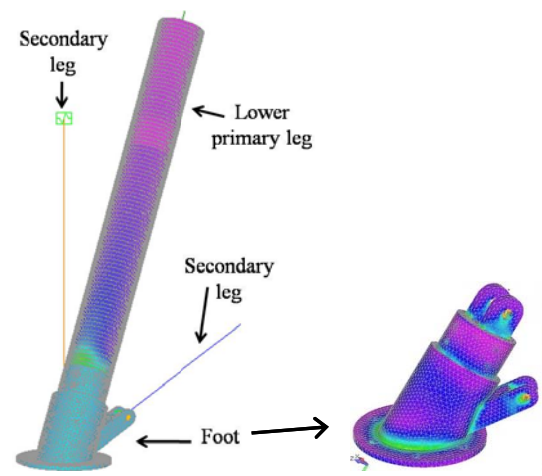

Fig. 19. Lower leg assembly and foot FEMAP models

Table 4. Lower leg margins of safety

Component	Material	Von Mises stress (kPa)	Yield stress (kPa)	Factor of safety	Margin of safety
Foot	Al 6061-T6	111,006	241,317	1.3	0.7
Lower Tube	Al 6061-T6	4,068	241,317	1.3	44.9

All component stress analysis results show positive margins for the design loads. Several components have exceedingly high margins, so the team will attempt to lightweight those parts in the next cycle of the design.

6. CONCLUSION AND FUTURE WORK

In conclusion, the RLL mechanical team has completed the preliminary design of a soft landing system for a lunar robotic probe. The team established requirements and conducted trades, based on the RLL mission architecture. After conducting some component development testing, a preliminary design was developed and analyzed for conformance to the requirements. The design was modified to also meet the requirements of the WGTA. Preliminary analyses indicate the design will perform well over the simulated conditions.

The next step in the landing leg development process is to validate the landing system-level analysis. Modifications are already under way to modify the drop test fixture to provide an interface for the 3-member leg assembly (see Fig. 20). A development unit leg will be fabricated, fully instrumented, and tested in a variety of landing conditions. Finally, a set of 3 landing legs will be fabricated and tested in the WGTA test program on the free flying vehicle.

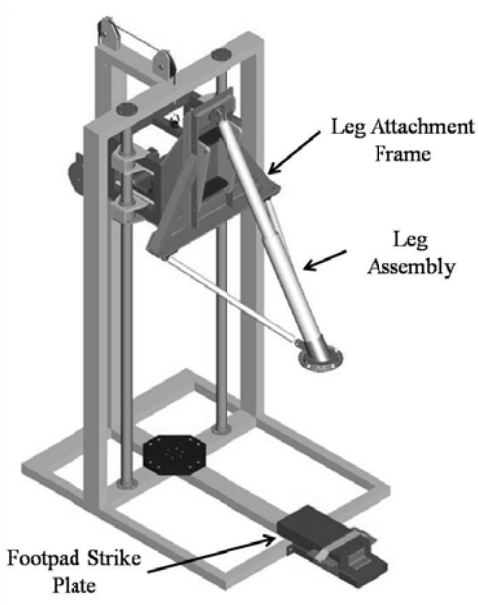

Fig. 20. Leg assembly drop test set-up

7. ACKNOWLEDGEMENTS

The authors gratefully acknowledge the support of the Robotic Lunar Lander Development Project office at MSFC and the MSFC/APL lander and WGTA design teams. Particular thanks go to Tim Cole, Bill French, Charlie Judge, Bob Matteson, Rick Startt, Ken Turner, and Jim Weber.

8. REFERENCES

1. Cohen B., et al, The International Lunar Network (ILN) Anchor Nodes Mission, Ground-based Geophysics on the Moon, Lunar and Planetary Science Conference, 2010, #3043.
2. Cohen B., et al, The International Lunar Network (ILN) Anchor Nodes Mission, 41st Lunar and Planetary Science Conference, 2010, #2616.
3. Walton W., Herr R. and Leonard H., Studies of Touchdown Stability for Lunar Landing Vehicles, *Journal of Spacecraft and Rockets*, Vol. 1, No. 5, 552-556, 1964.
4. Herr R. and Leonard H., Dynamic Model Investigation of Touchdown Stability of Lunar-Landing Vehicles, NASA TN D-4215, 1967.
5. Zupp G. and Doiron H., A Mathematical Procedure for Predicting the Touchdown Dynamics of a Soft-Landing Vehicle, NASA TN D-7045, 1971.
6. Hexcel Corporation, HexWeb Honeycomb Energy Absorption Systems Design Data, March 2006.